Desalination and Water Treatment
www.deswater.com

doi: 10.5004/dwt.2017.21101

84 (2017) 299–308
July

Oxygen depolarized cathode in advanced chlor-alkali cell with Pt–Ru nanoparticles as electro-catalyst: effect of process conditions and response surface methodology

Mir Ghasem Hosseini[a,b,*], Parisa Zardari[a]

[a]*Department of Physical Chemistry, Electrochemistry Research Laboratory, University of Tabriz, Tabriz, Iran, email: mg-hosseini@tabrizu.ac.ir*
[b]*Engineering Faculty, Department of Materials Science and Nanotechnology, Near East University, 99138 Nicosia, North Cyprus, Mersin 10, Turkey*

Received 18 February 2017; Accepted 25 June 2017

ABSTRACT

The effect of various operating parameters on the cell voltage of an advanced chlor-alkali membrane cell is studied. The optimization and modeling of the electrolysis process are performed through the response surface methodology (RSM) in combination with central composite design (CCD). The electrolysis process is carried out in the filter press advanced chlor-alkali membrane cell by using a half-MEA (Nafion® 115 membrane coated with Pt–Ru/MWCNTs) as the oxygen depolarized cathode and a dimensionally stable anode. Cell temperature, brine concentration, pH and current density are considered as input variables for RSM. The predicted values of cell voltage are found to be in good agreement with experimental values (R^2 = 0.9555 and Adj-R^2 = 0.9165). The optimization process show that the minimum cell voltage is achieved at the optimum conditions: cell temperature 80°C, brine concentration 320 g/L, pH 3.7 and current density 1 kA/m^2. Finally, the current density effect on the cell voltage and caustic current efficiency (CCE) of advanced chlor-alkali cell is studied under optimal conditions. The results show that by increasing the applied current density, the cell voltage is increased and CCE is decreased and reach to 2.27 V and 89.90% at 5 kA/m^2, respectively.

Keywords: Advanced chlor-alkali cell; Oxygen depolarized cathode; Pt–Ru/MWCNT catalyst; 1; Central composite design

1. Introduction

Sodium hydroxide and chlorine are produced by the electrolysis of brine in the chlor-alkali industry [1]. The brine electrolysis is performed by three methods included the mercury, diaphragm and ion-exchange membrane processes [2]. The brine electrolysis system has been changed from the mercury and the diaphragm process to the ion-exchange membrane process in the most advanced countries because of the attempting to reduce the manufacturing costs of chlorine production [3]. The total cell reaction proceeds through the following anodic and cathodic half-cell reactions:

$$2Cl^- \rightarrow Cl_2 + 2e^- \qquad E = +1.358 \text{ V/NEH} \tag{1}$$

$$2H_2O + 2e^- \rightarrow 2OH^- + H_2 \qquad E = -0.828 \text{ V/NHE} \tag{2}$$

The decomposition voltage (thermodynamic potential difference) of total electrode reactions is approximately 2.2 V [4]. The hydrogen evolution reaction (HER; Eq. (2)) occurs at the conventional cathode in the ion-exchange membrane brine electrolysis. However, the oxygen reduction reaction (ORR; Eq. (3)) takes place if the oxygen depolarized cathode (ODC) is used:

$$O_2 + 2H_2O + 4e^- \rightarrow 4OH^- \qquad E = +0.401 \text{ V/NHE} \tag{3}$$

* Corresponding author.

The equilibrium potential of the ORR is about 1.2 V/NHE higher than that of the HER [5]. Hence, by replacing the HER cathodes in a membrane cell with an ODC, the cell voltage and energy consumption can be reduced by as much as 30%–40% [6]. For effective ODC at the membrane cells, a high performance gas diffusion electrode (GDE) is required [7]. The GDE consists of a reaction layer, gas diffusion layer (GDL) and current distributor. The reaction layer structure is made of carbon black and an active catalyst. A key factor of GDE performance is the ORR at a reasonably low over-potential [8]. Many types of electro-catalysts for ORR have been investigated [9,10]. The best and standard catalyst routinely used as ORR in the GDEs is Pt/C [11]. The durability test of ODCs under the severe conditions of brine electrolysis indicated that the hot concentrated sodium hydroxide can oxidize the carbon carriers. The studies showed the higher long-term stability of carbon-free electrodes with silver as electro-catalyst [12]. Moreover, Pt metal, which is widely used as the electro-catalyst of ORR, is expensive, and its limited supply poses a serious problem in commercialization of chlor-alkali membrane cell technology. Many studies have been carried out to reduce this economical problem in recent decades [13]. Some efforts focused on the use of Pt-based alloys for solving this feature [14–16]. In our previous study, Pt–Ru/C nanoparticles were used as an ORR electro-catalyst of GDE [4]. As a result, Pt–Ru/C showed better electro-catalyst performance than Pt/C. Another effective way to enhance the catalytic activity of Pt-based alloying catalysts is to load the active particles onto nanomaterials as support catalysts. Recently, single wall nanotubes (SWNTs) and multi-walled carbon nanotubes (MWCNTs) have attracted much interest, due to their morphology and interesting properties such as nanometer size, high accessible surface area, better electronic conductivity and high stability [17]. However, it seems that Pt-based bimetallic catalysts deposited on MWCNTs can show synergistic catalytic activities toward ORR. In the present work, Pt-Ru/MWCNTs were used as ORR electro-catalyst of chlor-alkali membrane cell.

On the other hand, the chlorine production by the electrolysis of brine in the membrane cells is dependent on a number of parameters [18]. In the conventional methods used to determine the influence of operational parameters, experiments were carried out varying systematically the studied parameter and keeping constant the others. This should be repeated for all the influencing parameters, resulting in the numerous experiments. To optimize the effective parameters with the minimum number of experiments, the application of experimental design methodologies can be useful. Response surface methodology (RSM) is a statistical method being useful for the optimization of industrial processes and widely used for experimental design [19,20]. In this technique, the main objective is to optimize the response surface that is influenced by process parameters. RSM also quantifies the relationship between the controllable input parameters and the obtained response surface. Process optimization by RSM is faster for gathering experimental research results than the rather conventional, time-consuming one-factor-at-a-time approach [21].

The present work is focused on the Pt–Ru/MWCNT performance as an electro-catalyst of GDE in advanced chlor-alkali membrane cell. The central composite design (CCD) is applied to the optimization of the brine electrolysis. The factors investigated are the cell temperature, brine concentration, pH and applied current density.

2. Experimental procedure

2.1. Chemicals used

Sodium borohydride ($NaBH_4$, 96%), sodium hydroxide (NaOH, 99%), Vulcan carbon (XC-72R), sulfuric acid (H_2SO_4, 98%), hydrogen peroxide (H_2O_2, 30%), hydrochloric acid (HCl, 37%), phenolphthalein indicator and 2-propanol ($(CH_3)_2CHOH$, 99.99%) are received from Merck. Ruthenium trichloride anhydrous ($RuCl_3{\cdot}3H_2O$, 99%) and chloroplatinic acid hydrate ($H_2PtCl_6{\cdot}xH_2O$, 99.99%) are purchased from Cole-Parmer (United States) and Sigma-Aldrich (Germany), respectively. Polytetrafluoroethylene (PTFE, 99%), Nafion® solution (5 wt%) and carbon cloth are obtained from Sigma-Aldrich, Cobat and ELAT®, respectively. Multi-walled carbon nanotubes (MWCNTs, 99%) and sodium chloride (NaCl, ≥99.5%) are purchased from Neutrino (OH content: 3.06 wt%) and Dr. Mojallali Chemical Labs, Iran, respectively. DuPont™ Nafion® 115 is used as a membrane.

2.2. Preparation of ODC

2.2.1. Gas diffusion layer

In total, 30 mg Vulcan carbon (XC-72R) and 20 mg PTFE are dispersed into 10 mL 2-propanol:water (volume ratio = 3:1), ultrasonicated for 2 h. Then obtained suspension is painted onto the carbon cloth (geometric exposed area of 5 cm^2) and dried at 80°C. This method is repeated several times until the 1 mg cm^{-2} loading of painted ink is achieved. Finally, the painted carbon paper is dried at 120°C for 1 h and sintered at 340°C for 30 min.

2.2.2. Nafion membrane treatment

Nafion® 115 membrane is pre-cleaned in boiling water for 15 min, then boiled in 3% H_2O_2 solution for 30 min to remove organic impurities, after washing with distilled water it is boiled in 0.5 M H_2SO_4 for 30 min to exchange ions with protons, and again washed with distilled water. Prepared membrane is boiled in distilled water for 15 min three times and finally stored in distilled water until use.

2.2.3. Catalyst layer preparation

Approximately 40 mg of MWCNTs is ultrasonically dispersed into the 10 mL 2-propanol and water (volume ratio = 3:1), for 2 h. Metal precursors ($H_2PtCl_6{\cdot}xH_2O$ + $RuCl_3$) are added to the resulted MWCNTs ink. The molar ratio of Pt to Ru was chosen 1:1 and the results showed ORR catalytic enhancement in the compression of single Pt catalyst [4]. The total metal content in the electro-catalyst is 20 wt% vs. MWCNTs support. Finally, 10 mL of an aqueous solution of $NaBH_4$ in excess (stoichiometric metal:$NaBH_4$ ratio = 1:15, mol:mol) is added dropwise into the above solution under stirring at 80°C. The solid particles are separated from the solution by filtration, then washed and dried at 120°C for 6 h. The crystal structure is characterized by X-ray diffraction (XRD-6000)

using Cu K_α radiation (λ = 1.5416 Å) at the scale of 20°–90°. The surface morphology and composition of the catalyst is studied with a scanning electron microscope (Model XL30, Philips, United States) and energy dispersive X-ray (EDX) analysis, respectively. X-ray photoelectron spectroscopy (XPS) data are obtained with an ESCALab220i-XL electron spectrometer (VG Scientific, United States) using 300 W Al K_α radiations.

To prepare the catalyst ink, 18 mg of the catalyst is mixed with 3 mL deionized water, 7 mL 2-propanol and 0.5 mL Nafion® (5 wt%) and the mixture was ultrasonicated for 2 h. The loading of active metal catalyst ink onto the membrane is maintained at 0.5 mg cm^{-2} and the efficiency of spraying assumed to be 70%.

Prepared Nafion® 115 membrane is dried in the oven at 70°C for an hour between two sintered glass plates to avoid deformation during drying. Dried membrane is weighed out, then mounted in a 5 cm^2 frame and put on the hotplate at 80°C. The ink is carefully sprayed on the membrane using an air brush, and then it is left on the hotplate for 10 min to be dried. Then the membrane is put in the oven at 80°C for 15 min to make sure there is no water remains in the catalyst layer to interfere weight measurement. The membrane with catalyst is weighed out, and then subtracted to the membrane's weight to get the desired load. The painted membrane is put in the hot-press at 100°C for 1 min. The prepared GDL is put on the other side of the membrane, in the way that the painted side of carbon cloth attaches the membrane. Then the assembly is put in the hot-press at 130°C for 1 min and used as half-MEA.

2.3. Experimental setup

The electrochemical cell is a divided filter-press type made in laboratory (Fig. 1). The structural supports of advanced chlor-alkali membrane cell are made from polypropylene (Fig. 1(a)). The coated Nafion® membrane divides the anode side of the reactor from the cathode side. The anode is a dimensionally stable anode (DSA®, De Nora, Italy; Fig. 1(g)) and the cathode is prepared half-MEA (Fig. 1(d)). The anode flow field was made from ~2 mm Teflon® as a spacer (Fig. 1(f)). A particular graphite block having patterned channels for gas/liquid distribution is allocated right after the half-MEA (Fig. 1(c)). The electric current is directly connected to the anode (DSA®) and a copper plate used as current collector for the cathode side (Fig. 1(b)) [22–24]. The cell gaskets are made from silicon (Fig. 1(e)).

During the electrolysis, the anolyte is continuously fed into the jacketed heater anode chamber with a thermometer to monitor its temperature. Moreover, the anolyte pH is controlled by the feed pH. The anode and cathode chamber overflows are conducted to different separators for further depleted reactant separation and recirculation. The anolyte is prepared from analytical grade NaCl (≥99.5%) using deionized water and fed to the cell with a constant flow rate of 500 mL/h. The oxygen stream is heated and humidified by a laboratory made humidifier (HF) [25] and fed to the cathode side of the cell through graphite block [26]. The cathode chamber was fed with oxygen at 250 kPa with a flow rate corresponding to three times that required by stoichiometry of the four-electron oxygen reduction at the applied current density. Constant currents are applied to the cell and the corresponding cell voltages are measured by a multimeter. After each test, the setup was washed thoroughly with deionized water, drained and dried. Preliminary tests showed that the system reached steady-state conditions after 30 min. Therefore, the current density is applied after 30 min from the beginning of each experiment. Caustic current efficiency (CCE) is determined from titration of the obtained sodium hydroxide with standardized 1.0 M HCl solution against phenolphthalein indicator.

2.4. Experimental design

In this study, four factors are introduced as RSM input variables which their experimental ranges in coded and actual values are presented in Table 1. The coded values are applied for statistical calculations, according to the following equation [27]:

$$X_i = \frac{z_i - z_0}{\delta z} \tag{4}$$

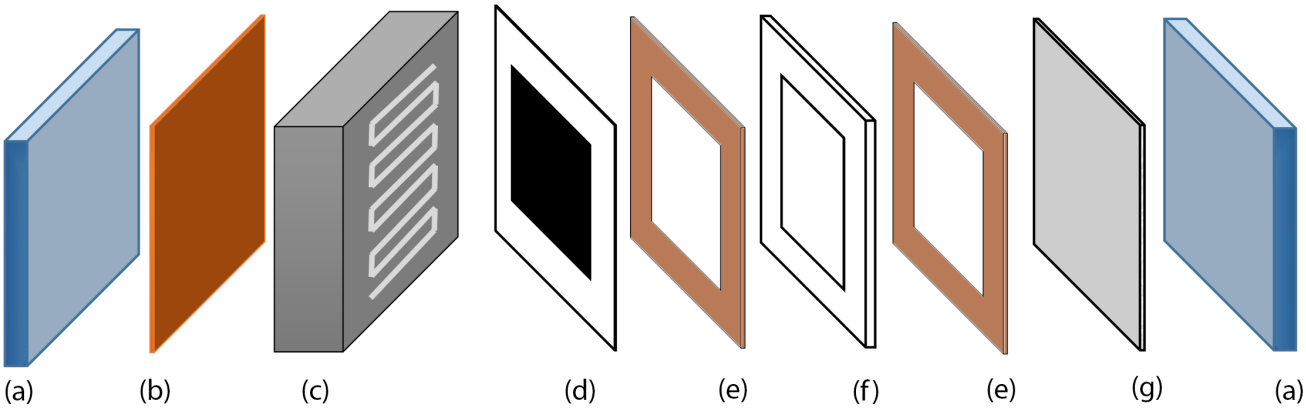

Fig. 1. Components of the advanced chlor-alkali membrane cell used in this study: (a) structural support polypropylene, (b) current distributor-copper, (c) gas distributor-graphite, (d) half-MEA, (e) gasket-silicon, (f) spacer-Teflon® and (g) anode-DSA®.

where X_i denotes the coded level of the variable (dimensionless value), z_i is the actual value of the variable, z_0 is the center point of the variable and δz is the interval variation. CCD is employed to evaluate the individual and interactive effects of four main controllable variables on the cell voltage (output response). CCD with four input variables consists of 31 experiments with 16 orthogonal two-level full factorial design points (coded as ±1), 8 axial points (or star point coded as ±2) and 7 replications of the central points to provide an estimation of the experimental error variance. The design of experiments and experimental data analysis are performed using Minintab 16 software. The design matrix of experiments is presented in Table 2.

Table 1
Experimental ranges and levels of the independent test variables

Variable	Ranges and levels				
	−2	−1	0	+1	+2
Cell temperature (°C) (X_1)	20	35	50	65	80
Brine concentration (g/L) (X_2)	200	230	260	290	320
pH (X_3)	2	3	4	5	6
Current density (kA/m^2) (X_4)	1	2	3	4	5

3. Results and discussion

3.1. Physical characterization and structural studies

XRD pattern of Pt–Ru/MWCNT catalysts is given in Fig. 2 and shows that the prepared catalyst has typical Pt fcc structure. The peak about 25.79° is related to the (200) reflection of the MWCNT structure [28]. The other four peaks are characteristic of fcc crystalline Pt, 40.25°, 47°, 68°, 82°. On the other hand, 2θ of (111) peak is shifted from 39.8° to 40.25°. The angle shift of Pt peak implies the alloy formation between Pt and Ru and incorporation of Ru

Table 2
The four-factor central composite design matrix and the value of response function (cell voltage, V)

Run	Cell temperature (°C)	Brine concentration (g/L)	pH	Current density (kA/m^2)	Cell voltage (V)	
					Experimental	Predicted
1	0	0	0	0	2.09	2.09
2	−1	+1	+1	+1	2.32	2.35
3	0	−2	0	0	2.11	2.07
4	−1	−1	−1	+1	2.20	2.22
5	0	0	0	0	2.09	2.09
6	0	+2	0	0	2.07	2.10
7	0	0	0	0	2.09	2.09
8	+1	+1	+1	−1	1.89	1.88
9	0	0	+2	0	2.30	2.21
10	0	0	0	0	2.09	2.09
11	+1	−1	−1	+1	2.21	2.19
12	+2	0	0	0	1.97	1.97
13	−2	0	0	0	2.23	2.22
14	+1	−1	+1	−1	1.89	1.92
15	0	0	0	0	2.09	2.09
16	0	0	0	−2	1.78	1.81
17	−1	+1	−1	−1	2.08	2.05
18	0	0	−2	0	2.00	2.08
19	+1	+1	−1	−1	1.87	1.84
20	−1	−1	−1	−1	2.00	1.97
21	0	0	0	+2	2.43	2.39
22	−1	+1	−1	+1	2.32	2.29
23	0	0	0	0	2.09	2.09
24	−1	−1	+1	+1	2.29	2.31
25	+1	−1	+1	+1	2.22	2.27
26	+1	−1	−1	−1	1.88	1.86
27	+1	+1	+1	+1	2.20	2.22
28	+1	+1	−1	+1	2.19	2.17
29	0	0	0	0	2.09	2.09
30	−1	−1	+1	−1	2.02	2.05
31	−1	+1	+1	−1	2.09	2.10

atoms on Pt lattice [29]. The lattice parameter for fcc phase of Pt is 0.3902 nm.

The SEM images and EDX analysis of Pt–Ru/MWCNTs are shown in Fig. 3. SEM image shows plenty of nanotube tangles together with some particles clinging to them. In the other words, the MWCNT surfaces form densely packed rod-shaped carbon clusters and are coupled with the sphere-shaped nanoparticles on them. The EDX analysis reveals the presence of 9.15 and 10.81 wt% Pt and Ru, respectively. The obtained weight percentage of Pt and Ru is in good agreement with nominal values of catalyst.

XPS spectra of Pt–Ru/MWCNTs are recorded to study the chemical state of Pt and Ru in nanocatalyst. Fig. 4 shows the XPS spectra of Pt 4f and Ru 3d in the Pt–Ru/MWCNT catalyst. The Pt 4f spectra is deconvoluted into the doublets of 7/2 and 5/2, and each doublet consisted of Pt^0 and Pt^{2+} species as shown in Fig. 4(a). The Pt^0 peaks are obtained at the binding energies of 71.6 and 74.9 eV, which are related to Pt $4f_{7/2}$ and Pt $4f_{5/2}$, respectively. In Fig. 4(b), the XPS spectrum of Ru 3d shows the Ru $3d_{5/2}$ peak at 280.9 eV. The overlapping of the C 1s and the Ru $3d_{3/2}$ peaks at ~285 eV makes it complicated to assign the binding energy of Ru $3d_{3/2}$. For C 1s spectrum of MWCNTs, the peaks at 285.7 and 288.7 are attributed to C–C and C–OOH groups, respectively.

Cross-sectional SEM image of the painted membrane is shown in Fig. 5. There are two distinct layers in the SEM image. A thin film comprised of Pt–Ru/MWCNT catalyst layer is observed at the surface and the under layer is a structural membrane base. The thickness of the thin catalyst layer on the membrane support is calculated from the cross-sectional SEM image. It is observed that the average thickness of catalyst layer is ~16 μm.

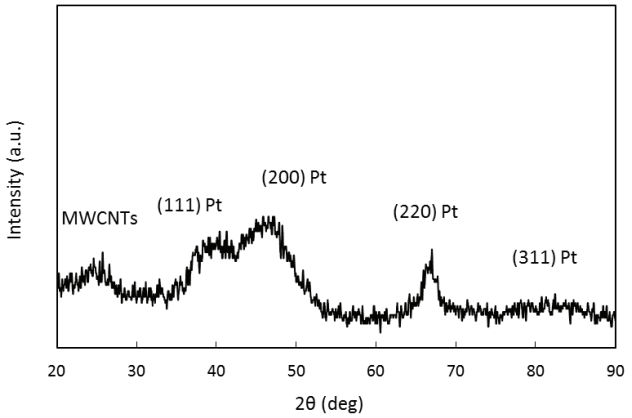

Fig. 2. XRD pattern of Pt–Ru/MWCNT catalyst.

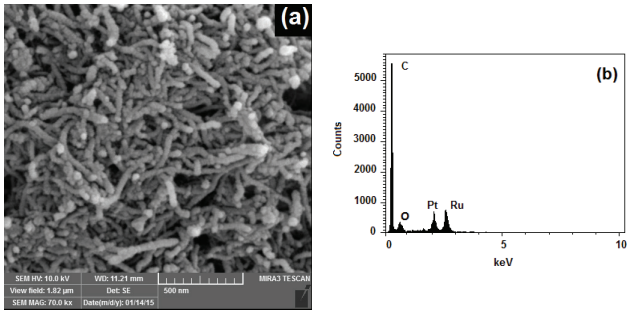

Fig. 3. SEM images (a) and EDX analysis (b) of Pt–Ru/MWCNT catalyst.

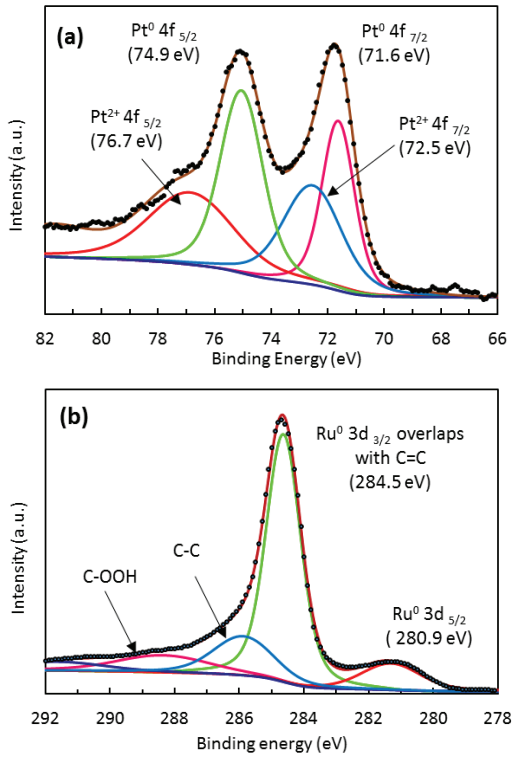

Fig. 4. XPS spectra of Pt 4f (a), Ru 3d and C 1s (b) in the Pt–Ru/MWCNT catalyst.

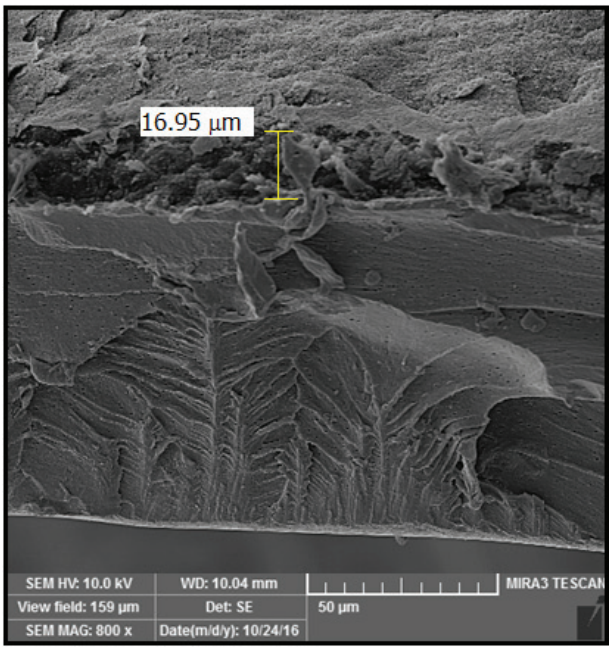

Fig. 5. Cross-section SEM image of Pt-Ru/MWCNT thin-film coated on the membrane.

3.3. CCD model and residuals analysis

A second-order (quadratic) polynomial response surface model (Eq. (5)) is applied to fit the experimental results obtained by CCD. This model describes a polynomial approximation of experimental results with following relationship:

$$Y = b_0 + \sum_{i=1}^{n}(b_i X_i) + \sum_{i=1}^{n}(b_{ii} X_{ii}^2) + \sum_{i,j=1}^{n}(b_{ij} X_i X_j) \quad (5)$$

where Y is the predicted response, X_i indicates the coded experimental levels of the variable, b_0 is a constant and b_i, b_{ii} and b_{ij} are the regression coefficients for the linear, quadratic and interaction effects, respectively [30].

Based on these results, the empirical relationship between the response and independent variables is attained and expressed by the following equation:

$$\begin{aligned} Y = {} & 2.09000 - 0.06208x_1 + 0.00708x_2 + 0.03208x_3 \\ & + 0.14708x_4 + 0.00135x_1^2 - 0.00115x_2^2 + 0.01385x_3^2 \\ & + 0.00260x_4^2 - 0.02187x_1x_2 - 0.00437x_1x_3 + 0.02188x_1x_4 \\ & - 0.00563x_2x_3 - 0.00188x_2x_4 + 0.00313x_3x_4 \end{aligned} \quad (6)$$

The voltage of advanced chlor-alkali cell is predicted by Eq. (6) and presented in Table 2. These results indicate the good agreements between the experimental and predicted values of cell voltages. The significance and adequacy of the model are evaluated by analysis of variance (ANOVA) and the obtained results are shown in Table 3.

The correlation coefficient (R^2) quantitatively evaluates the correlation between the experimental data and the predicted responses. It was found that the predicted values matched the experimental values reasonably well with R^2 = 0.9555. It means that the 95.55% of the variations in cell voltages are explained by the proposed model and only 4.45% of variations cannot be explained by model. Adjusted R^2 (Adj-R^2) is also a measure of the goodness of a fit and it is more suitable for comparing models with different numbers of independent variables. If there are many terms in a model and not very large sample size, Adj-R^2 may be visibly smaller than R^2 [31]. The value of Adj-R^2 is found to be 0.9165 which is very close to the corresponding R^2 value (Table 3).

In addition to the mentioned criteria for evaluating the adequacy of the models, the difference between experimental and predicted responses (residuals) can be used for investigating the adequacy of the model. Residuals are thought as elements of variation unexplained by the fitted model and they will occur based on a normal distribution, if the model is a good predictor [32]. In Fig. 6, normal probability plots of residuals (Fig. 6(a)) and residuals vs. fit plots (Fig. 6(b)) are shown for the processes describing models. Trends observed in Fig. 6 reveal reasonably well-behaved residuals. Based on these plots, the residuals appear to be randomly scattered. On the other hand, ANOVA subdivides the total variation of the results into two components: variation associated with the model and variation associated with the experimental error. The ratio between the mean square of the model and the residual error is defined as F value. If the model is a good predictor of the experimental results, F value should be greater than the tabulated value [33]. Here, F value obtained is 24.53, which is clearly greater than the tabulated F (2.352 at the 95% significance) and confirming the adequacy of the model fits.

Table 3
Analysis of variance (ANOVA) for fit of cell voltage from central composite design

Source of variation	Regression	Residual	Total
Sum of squares	0.659697	0.030742	0.690439
Degrees of freedom	14	16	30
Adjusted mean square	0.047121	0.001921	
F value	24.53		
R^2 = 0.9555, Adj-R^2 = 0.9165			

3.4. Determination of importance of model terms

The Student's t distribution and the corresponding values, along with the parameter estimate, are given in Table 4 to determine the effective terms of the developed model. The greater T value and the smaller p value (less than 0.05 at the 95% significance) for a coefficient indicate the most significant influence of it [34].

The coefficient with p value greater than 0.05 are eliminated and Eq. (6) is rewritten as follows:

$$Y = 2.09000 - 0.06208x_1 + 0.03208x_3 + 0.14708x_4 \quad (7)$$

In addition, the Pareto analysis can be applied to determine the significance of each factor. According to this analysis the percentage effect of each factor (P_i) on the response can be calculated as follows [35]:

$$P_i = \left(\frac{b_i^2}{\sum_{i=1}^{n} b_i^2}\right) \times 100 \qquad i \neq 0 \quad (8)$$

The Pareto graphic analysis is shown in Fig. 7. The results indicate that among the variables, current density (77.85%) and cell temperature (13.87%) produce the highest effect on voltages of advanced chlor-alkali cell.

3.5. Effects of variables on the cell voltage

As concluded above, the current density and the cell temperature are the most important factors in cell voltage. Fig. 8 illustrates three-dimensional response surface and two-dimensional counter plot for investigating the interactions between the variables. The X- and Y-axis values of these figures are the real values. The results demonstrate that the cell voltage is increased sharply by increasing the applied current density and the trend of cell voltage increase is very close to be linear [36]. The effect of brine concentration indicates that at higher temperature and current density, the cell voltage is decreased by increasing the higher brine concentration. The effect of temperature on the cell performance was studied and the results show that the increasing of cell temperature reduces the cell voltage. At higher temperatures, the higher conductivity of solution lowers the cell voltage and reduces the energy consumption of the cell [19]. In addition, increasing of cell temperature improves the reaction kinetics and

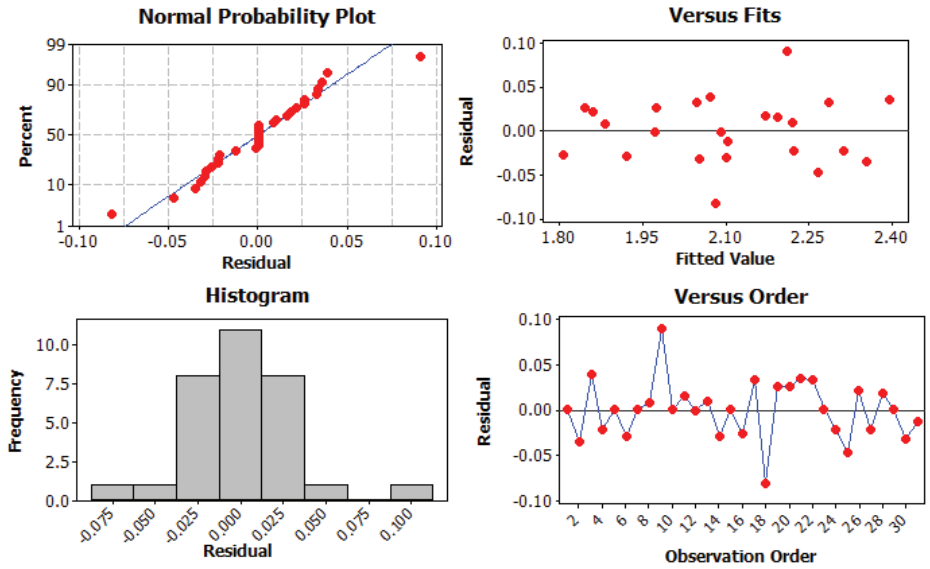

Fig. 6. Residual plots for cell voltage of advanced chlor-alkali cell.

Table 4
Estimated regression coefficient and corresponding T and p values from the data of central composite design experiments

Coefficient	Coefficient estimate	T value	p value
b_0	2.09000	126.151	0.000
b_1	−0.06208	−6.939	0.000
b_2	0.00708	0.792	0.440
b_3	0.03208	3.586	0.002
b_4	0.14708	16.439	0.000
b_{11}	0.00135	0.165	0.871
b_{22}	−0.00115	−0.140	0.891
b_{33}	0.01385	1.690	0.110
b_{44}	0.00260	0.318	0.755
b_{12}	−0.02187	−1.996	0.063
b_{13}	−0.00437	−0.399	0.695
b_{14}	0.02188	1.996	0.063
b_{23}	−0.00563	−0.513	0.615
b_{24}	−0.00188	−0.171	0.866
b_{34}	0.00313	0.285	0.779

lowers the Gibbs free energy and therefore, decrease cell voltage [37]. On the other hand, the cell voltage increases at higher pHs. It is due to the production of by-products such as hypochlorite and chlorate in brine at higher pHs [38]. However, if the pH is kept too low, the competition of H^+ and Na^+ concerning carrying the charge will be high [39].

3.6. Determination of optimal conditions for cell voltage

The quadratic models obtained by the RSM can be used to optimize and minimize the cell voltage. In order to confirm the reliability of the model established in this study, the validation experiments are performed three times under the operating conditions predicted by the model for minimum cell voltage. The optimum values of the process variables for the minimum cell voltage are 80°C, 320 g/L, 3.7 and 1.0 kA/m^2 for cell temperature (X_1), brine concentration (X_2), pH (X_3) and current density (X_4), respectively. At these optimum conditions, the predicted and observed three cell voltages are 1.53 and 1.58, 1.56, 1.60 V, respectively. It implies that the strategy to optimize the cell performance and to obtain the minimum voltage by RSM is successful.

3.7. Advanced chlor-alkali cell performance under optimal conditions

The brine electrolysis is carried out under optimal conditions and different current densities in the advance chlor-alkali cell. The current density effect on the cell voltage and CCE is shown in Fig. 9. The CCE is calculated based on the following equation [40]:

$$\text{CCE} = \text{NaOH moles produced}/(It/nF) \quad (9)$$

where I is current (A), t indicates the electrolysis time (s), n is the number of transferred electron and F is Faraday number (C/mol).

As it can be seen by increasing the current density, the cell voltage is increased and it is obtained 2.27 V at 5 kA/m^2 which is in good agreement with Eq. (6) at optimal conditions (T = 80°C, brine concentration = 320 g/L and pH = 3.7). A comparison of the obtained cell voltages with literature data shows that the prepared half-MEA electrode is in most cases superior to other ODCs. The cell voltage of 2.0 V at 3 kA/m^2 has been reported by Saiki et al. (2 mm catholyte gap) [41]. Nakamatsu and coworkers [42] have measured 2.14 V at 3 kA/m^2, 80°C, 7 mm catholyte gap. The cell voltage of 2.05 V at 3 kA/m^2 and 90°C in a zero gap cathode arrangement has been reported by Ashida and coworkers [43]. While the cell voltage of prepared Pt–Ru/MWCNT ODC in optimal conditions and the current density of 3 kA/m^2 is 1.89 V (Fig. 9).

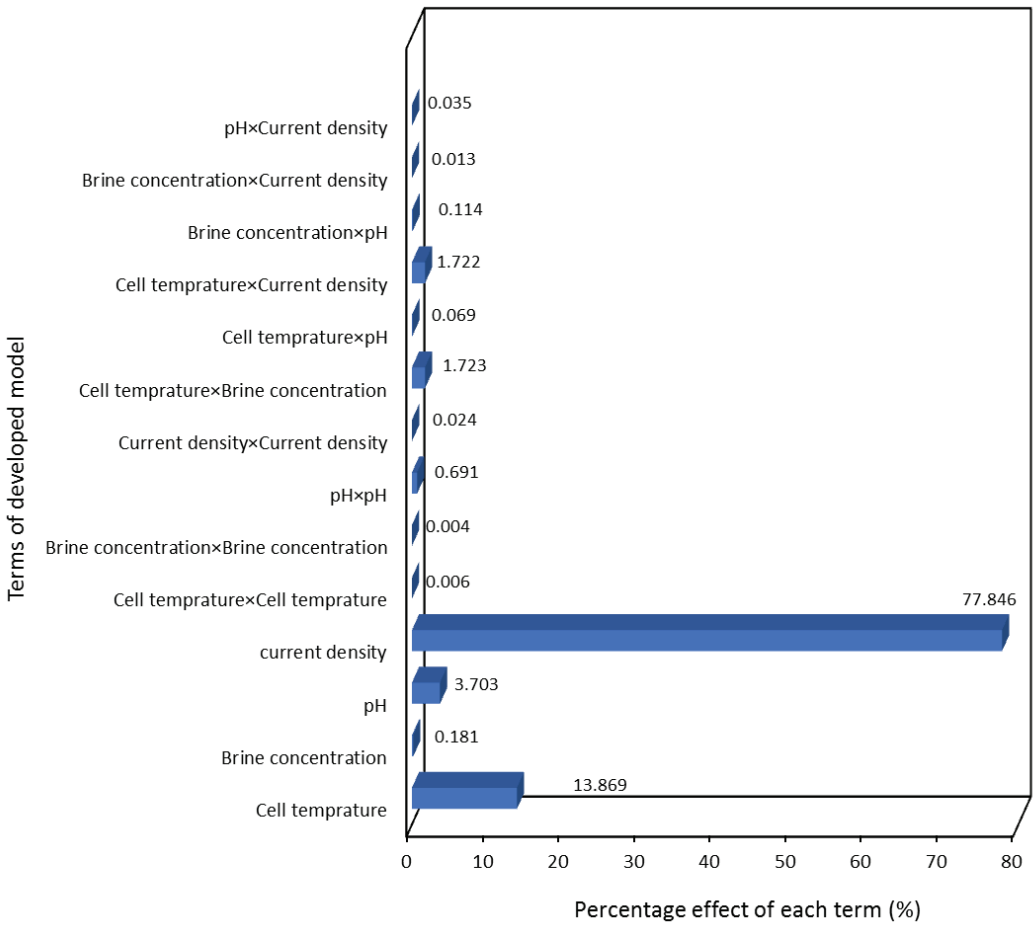

Fig. 7. Pareto graphic analysis of cell voltage.

The CCE decreases with increasing the applied current density (Fig. 9). This is as a result of different ORR kinetics which can be happened by four-electron transfer or undesired two-electron transfer pathways:

$$O_2 + 2H_2O + 4e^- \rightarrow 4OH^- \qquad E = +0.401 \text{ V/NHE} \qquad (10)$$

$$O_2 + H_2O + 2e^- \rightarrow OOH^- + OH^- \qquad E = -0.065 \text{ V/NHE} \qquad (11)$$

The increase of current density causes to cathode potential shifts towards the more negative potentials and can affect the rates of Eqs. (10) and (11). Reaction (10) is more favorable than Reaction (11) because of four hydroxyl ion production per every oxygen molecule [44].

For the ODCs, the cell voltage as a function of current density can be analyzed with the following equation:

$$V = a + kI \qquad (12)$$

where the rest voltage (a) is the extrapolated axis intercept at a current density of zero while the slope k, which is known as k factor, is a measure of all resistive processes in the cell, that is, ohmic resistances in electrode, membrane and oxygen mass transport resistances [45]. The k factor of Pt–Ru/MWCNT ODC at the present advanced chlor-alkali cell is calculated 0.171 V m^2/kA. Moussallem and coworkers have studied Ag-based GDE as an ODC in membrane chlor-alkali cell in a finite gap arrangement and the k factor of Ag-based ODC has been reported 0.174 V m^2/kA at optimal condition (Ag content: 98 wt% and 200 mg/cm^2 loading) [12].

4. Conclusions

The Pt–Ru/MWCNT electro-catalyst is prepared by chemical reduction process and coated on Nafion® 115 membrane. The coated membrane is used as half-MEA ODC in the advanced chlor-alkali cell. The effect of operating parameters including cell temperature (20°C–80°C), brine concentration (200–320 g/L), pH (2–6) and current density (1–5 kA/m^2) on the cell voltage of a laboratory made chlor-alkali cell is investigated by RSM. A high coefficient of determination (R^2 = 0.9555 and Adj-R^2 = 0.9165) between experimental and predicted cell voltages is achieved. The minimum cell voltage of advanced chlor-alkali cell is obtained by CCD under optimum conditions (cell temperature 80°C, brine concentration 320 g/L, pH 3.7 and current density 1.0 kA/m^2). The cell voltage and CCE are studied under optimal conditions and different applied current densities. At 5 kA/m^2, the cell voltage and CCE are achieved 2.27 V and 89.90%, respectively.

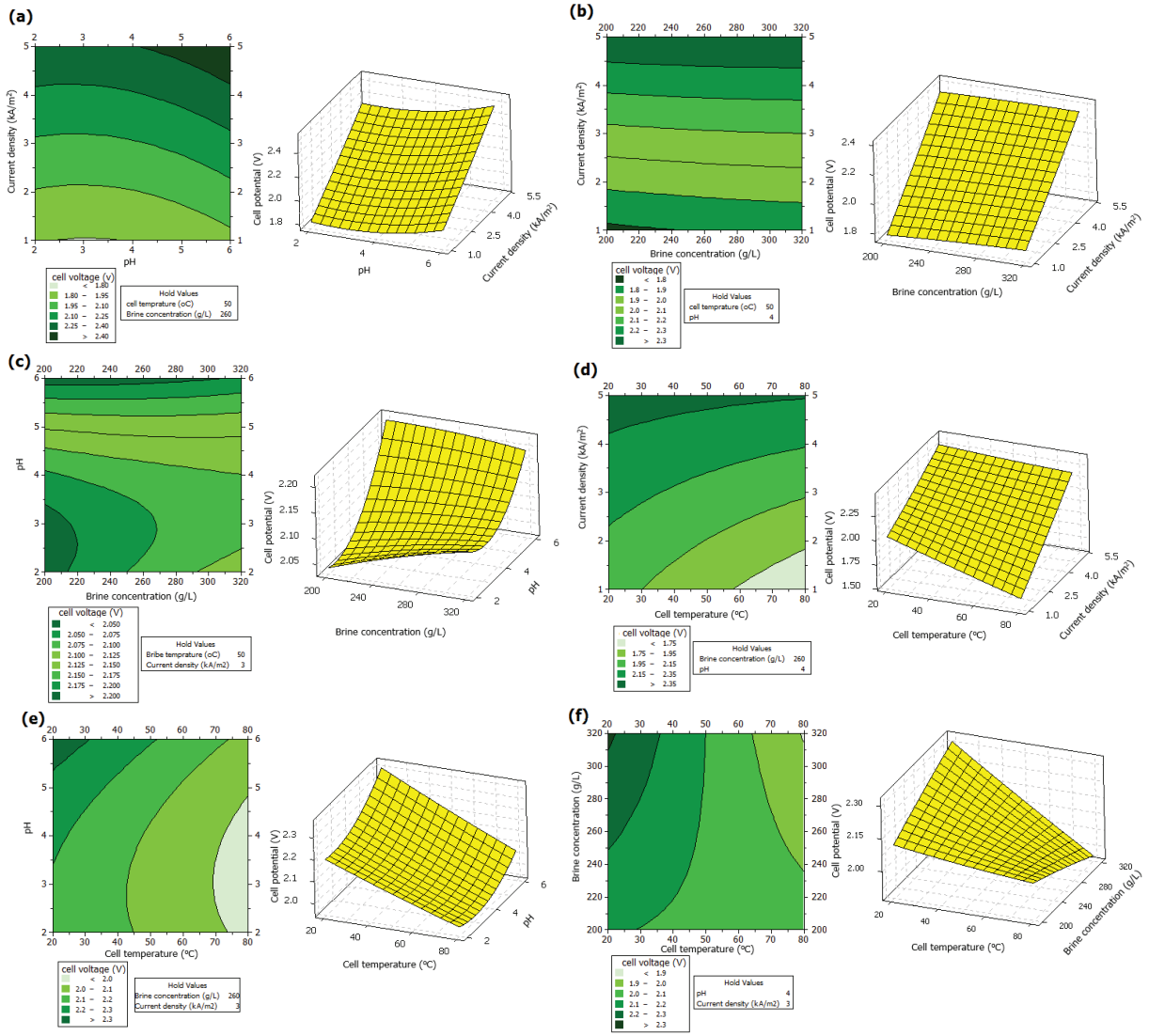

Fig. 8. The response surface and counter plots of cell voltage as a function of (a) pH and current density (kA/m^2), (b) brine concentration (g/L) and current density (kA/m^2), (c) brine concentration (g/L) and pH, (d) cell temperature (°C) and current density (kA/m^2), (e) cell temperature (°C) and pH, (f) cell temperature (°C) and brine concentration (g/L).

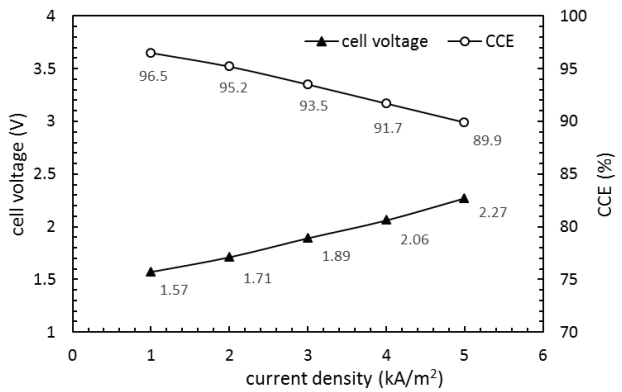

Fig. 9. The effect of current density on cell voltage (V) and CCE of the advanced chlor-alkali cell under optimal conditions (cell temperature 80°C, brine concentration 320 g/L and pH 3.7).

Acknowledgment

The authors would like to acknowledge the financial support of the Office in Charge of Research of Iranian Nanotechnology Society and the financial support of the Office of Vice Chancellor in charge of research of University of Tabriz.

References

[1] K. Mitko, W. Mikołajczak, M. Turek, Electrodialytic concentration of NaCl for the chlor-alkali industry, Desal. Wat. Treat., 56 (2015) 3174–3180.

[2] J.S. Ryu, J.Y. Jeong, J.H. Shim, Ji.Y. Park, Jo.Y. Park, Performance evaluation of diaphragm electrolysis cell for alkali production, Desal. Wat. Treat., 57 (2016) 24697–24703.

[3] E. Joudaki, F. Mohammadi, A. Yousefi, T. Mirzazadeh, Prediction of chlor-alkali's caustic current efficiency by artificial neural network; case study: a zero-gap advanced chlor-alkali cell, Desal. Wat. Treat., 8 (2009) 100–108.

[4] M.G. Hosseini, P. Zardari, Electrocatalytical study of carbon supported Pt, Ru and bimetallic Pt–Ru nanoparticles for oxygen reduction reaction in alkaline media, Appl. Surf. Sci., 345 (2015) 223–231.
[5] F. Gestermanna, A. Ottaviani, Chlorine Production with Oxygen-Depolarised Cathodes on an Industrial Scale, Modern Chlor-Alkali Technology, Blackwell Science Ltd., 2007, pp. 49–56.
[6] N. Shojaikaveh, S.N. Ashrafizadeh, Development and comparison of non-parameter regression methods for prediction of cell voltage and current efficiency in a lab scale chlor-alkali membrane cell, Desal. Wat. Treat., 14 (2010) 135–145.
[7] P. Mazur, J. Malis, M. Paidar, J. Schauer, K. Bouzek, Preparation of gas diffusion electrodes for high temperature PEM-type fuel cells, Desal. Wat. Treat., 14 (2010) 101–105.
[8] S. Chabi, M. Kheirmand, Electrocatalysis of oxygen reduction reaction on Nafion/platinum/gas diffusion layer electrode for PEM fuel cell, Appl. Surf. Sci., 257 (2011) 10408–10413.
[9] M. Oezaslan, F. Hasché, P. Strasser, $PtCu_3$, PtCu and Pt_3Cu alloy nanoparticle electrocatalysts for oxygen reduction reaction in alkaline and acidic media, J. Electrochem. Soc., 159 (2012) B444–B454.
[10] M. Hezarjaribi, M. Jahanshahi, A. Rahimpour, M. Yaldagard, Gas diffusion electrode based on electrospun Pani/CNF nanofibers hybrid for proton exchange membrane fuel cells (PEMFC) applications, Appl. Surf. Sci., 295 (2014) 144–149.
[11] S. Mukerjee, S. Srinivasan, Enhanced electrocatalysis of oxygen reduction on platinum alloys in proton exchange membrane fuel cells, J. Electroanal. Chem., 357 (1993) 201–224.
[12] I. Moussallem, S. Pinnow, N. Wagner, T. Turek, Development of high-performance silver-based gas-diffusion electrodes for chlor-alkali electrolysis with oxygen depolarized cathodes, Chem. Eng. Process., 52 (2012) 125–131.
[13] N. Jha, A. Leela Mohana Reddy, M.M. Shaijumon, N. Rajalakshmi, S. Ramaprabhu, Pt–Ru/multi-walled carbon nanotubes as electrocatalysts for direct methanol fuel cell, Int. J. Hydrogen Energy., 33 (2008) 427–433.
[14] K. Jayasayee, J.A.R.V. Veen, T.G. Manivasagam, S. Celebi, E.J.M. Hensen, F.A. de Bruijn, Oxygen reduction reaction (ORR) activity and durability of carbon supported PtM (Co, Ni, Cu) alloys: influence of particle size and non-noble metals, Appl. Catal. B., 111–112 (2012) 515–526.
[15] G. Sievers, S. Mueller, A. Quade, F. Steffen, S. Jakubith, A. Kruth, V. Brueser, Mesoporous Pt–Co oxygen reduction reaction (ORR) catalysts for low temperature proton exchange membrane fuel cell synthesized by alternating sputtering, J. Power Sources, 268 (2014) 255–260.
[16] I.E. Pech-Pech, D.F. Gervasio, J.F. Pérez-Robles, Nanoparticles of Ag with a Pt and Pd rich surface supported on carbon as a new catalyst for the oxygen electroreduction reaction (ORR) in acid electrolytes: Part 2, J. Power Sources, 276 (2015) 374–381.
[17] M.G. Hosseini, P. Zardari, Electrocatalysis of oxygen reduction on multi-walled carbon nanotube supported Ru-based catalysts in alkaline media, Int. J. Hydrogen Energy., 41 (2016) 8803–8818.
[18] F. Mohammadi, S.N. Ashrafizadeh, A. Sattari, Aqueous HCl electrolysis utilizing an oxygen reducing cathode, Chem. Eng. J., 155 (2009) 757–762.
[19] S.M. Ghoreishian Khashayar Badii, M. Norouzi Kaveh Malek, Effect of cold plasma pre-treatment on photocatalytic activity of 3D fabric loaded with nano-photocatalysts: application of response surface methodology, Appl. Surf. Sci., 365 (2016) 252–262.
[20] M.S. Seyed Dorraji, M.H. Rasoulifard, A.R. Amani-Ghadim, M.H. Khodabandeloo, M. Felekari, M.R. Khoshrou, I. Hajimiri, Microwave absorption properties of polypyrrole-$SrFe_{12}O_{19}$-TiO_2-epoxy resin nanocomposites: optimization using response surface methodology, Appl. Surf. Sci., 383 (2016) 9–18.
[21] N. Aslan, Application of response surface methodology and central composite rotatable design for modeling and optimization of a multi-gravity separator for chromite concentration, Powder Technol., 185 (2008) 80–86.
[22] T. Shimamune, K. Aoki, M. Tanaka, K. Hamaguchi, Y. Nishiki, Electrolytic Cell Employing Gas Diffusion Electrode, US Patent No. 6117286 2000.
[23] D. Pouli, L.S. Melnicki, E.J. Rudd, Electrolytic Cell Having a Depolarized Cathode, US Patent No. 4332662, 1982.
[24] M.L. Perry, Oxygen-Consuming Zero-Gap Electrolysis Cells with Porous/Solid Plates, US Patent No. 20100314261, 2010.
[25] L. Han, Method and system for near saturation humidification of a gas flow, US Patent No. 6988717, 2006.
[26] L. Lipp, S. Gottesfeld, J. Chlistunoff, Peroxide formation in a zero-gap chlor-alkali cell with an oxygen-depolarized cathode, J. Appl. Electrochem., 35 (2005) 1015–1024.
[27] G. Chen, J. Chen, C. Srinivasakannan, J. Peng, Application of response surface methodology for optimization of the synthesis of synthetic rutile from titania slag, Appl. Surf. Sci., 258 (2012) 3068–3073.
[28] Y. Zhao, L. Fan, J. Ren, B. Hong, Electrodeposition of Pt–Ru and Pt–Ru–Ni nanoclusters on multi-walled carbon nanotubes for direct methanol fuel cell, Int. J. Hydrogen Energy., 39 (2014) 4544–4557.
[29] E. Antolini, Formation of carbon-supported PtM alloys for low temperature fuel cells: a review, Mater. Chem. Phys., 78 (2003) 563–573.
[30] A. Abaamrane, S. Qourzal, M. El Ouardi, S. Alahiane, M. Belmouden, H. Bari, N. Barka, S. Mançour Billah, A. Assabbane, Y. Ait-Ichou, Modeling of photocatalytic mineralization of phthalic acid in TiO_2 suspension using response surface methodology (RSM), Desalin. Wat. Treat., 53 (2015) 249–256.
[31] M. Zarei, A. Niaei, D. Salari, A. Khataee, Application of response surface methodology for optimization of peroxi-coagulation of textile dye solution using carbon nanotube–PTFE cathode, J. Hazard. Mater., 173 (2010) 544–551.
[32] L.A. Sarabia, M.C. Ortiz, 1.12: Response Surface Methodology A2 – Brown, Steven D, R. Tauler, B. Walczak, Eds., Comprehensive Chemometrics, Elsevier, Oxford, 2009, pp. 345–390.
[33] S.A. Hassanzadeh-Tabrizi, Optimization of the synthesis parameters of high surface area ceria nanopowder prepared by surfactant assisted precipitation method, Appl. Surf. Sci., 257 (2011) 10595–10600.
[34] J.A. Cornell, Response Surfaces: Designs and Analyses, Marcel Dekker, Inc., 1987.
[35] M. Ji, X. Su, Y. Zhao, W. Qi, Y. Wang,G. Chen, Z. Zhang, Effective adsorption of Cr(VI) on mesoporous Fe-functionalized Akadama clay: optimization, selectivity, and mechanism, Appl. Surf. Sci., 344 (2015) 128–136.
[36] F. Hine, M. Nozaki, Y. Kurata, Bench scale experiment of recovery of chlorine from waste gas, J. Electrochem. Soc., 131 (1984) 2834–2839.
[37] F.R. Minz, Process for Performing HCl-Membrane Electrolysis, US Patent No. 4725341, 1988.
[38] A.A. Jalali, F. Mohammadi, S.N. Ashrafizadeh, Effects of process conditions on cell voltage, current efficiency and voltage balance of a chlor-alkali membrane cell, Desalination, 237 (2009) 126–139.
[39] J. Balster, D.F. Stamatialis, M. Wessling, Electro-catalytic membrane reactors and the development of bipolar membrane technology, Chem. Eng. Process., 43 (2004) 1115–1127.
[40] R.R. Chandran, D.T. Chin, Reactor analysis of a chlor—alkali membrane cell, Electrochim. Acta., 31 (1986) 39–50.
[41] K. Saiki, A. Sakata, H. Aikawa, N. Furuya, Reduction in Power Consumption of Chlor-alkali Membrane Cell Using Oxygen Depolarized Cathode, The Electrochemical Society Proceedings, 1999, pp. 188–195.
[42] S. Nakamatsu, K. Sakata, H. Aikawa, N. Furuya, Liquid-Permeable Gas Diffusion Electrode for Chlor-alkali Membrane Cells, The Electrochemical Society Proceedings, 1999, pp. 196–208.
[43] S.W.T. Ashida, M. Tanaka, Y. Nishiki, T. Shimamune, Chlor-alkali electrolysis with a zero-gap type oxygen cathode, Denki Kagaku 65 (1997) 1026–1031.
[44] P.S.D. Brito, C.A.C. Sequeira, Cathodic oxygen reduction on noble metal and carbon electrodes, J. Power Sources, 52 (1994) 1–16.
[45] S. Pinnow, N. Chavan, T. Turek, Thin-film flooded agglomerate model for silver-based oxygen depolarized cathodes, J. Appl. Electrochem., 41 (2011) 1053–1064.